MITSUBISHI ELECTRIC RESEARCH LABORATORIES
https://www.merl.com

Spatio-Temporal Thermal Monitoring for Lithium-Ion Batteries via Kriged Kalman Filtering

Tu, Hao; Wang, Yebin; Li, Xianglin; Fang, Huazhen

TR2022-162 December 09, 2022

Abstract

Thermal monitoring plays an essential role in ensuring safe, efficient and long-lasting operation of lithium- ion batteries (LiBs). Existing methods in the literature mostly rely on physics-based thermal models. However, an accurate physical thermal model is practically hard to obtain due to the existence of system uncertainties, such as uncaptured dynamics, parameter errors, and unknown cooling conditions. Motivated by this problem, this paper considers a data-driven approach named Kriged Kalman filter for estimating the temperature field of LiBs. First, we demonstrate that the evolution of a pouch-type LiB cell's temperature can be formulated in a physically consistent manner as a spatio-temporal random field. Then, we leverage the Kridged Kalman filter to update and reconstruct the random temperature field sequentially through time. Our simulations show that the proposed approach can provide accurate reconstruction of a LiB cell's temperature field with a small number of sensors.

IEEE Conference on Decision and Control (CDC) 2022

Mitsubishi Electric Research Laboratories, Inc.
201 Broadway, Cambridge, Massachusetts 02139

Spatio-Temporal Thermal Monitoring for Lithium-Ion Batteries via Kriged Kalman Filtering

Hao Tu[1], Yebin Wang[2], Xianglin Li[3], Huazhen Fang[1]

***Abstract*— Thermal monitoring plays an essential role in ensuring safe, efficient and long-lasting operation of lithium-ion batteries (LiBs). Existing methods in the literature mostly rely on physics-based thermal models. However, an accurate physical thermal model is practically hard to obtain due to the existence of system uncertainties, such as uncaptured dynamics, parameter errors, and unknown cooling conditions. Motivated by this problem, this paper considers a data-driven approach named Kriged Kalman filter for estimating the temperature field of LiBs. First, we demonstrate that the evolution of a pouch-type LiB cell's temperature can be formulated in a physically consistent manner as a spatio-temporal random field. Then, we leverage the Kridged Kalman filter to update and reconstruct the random temperature field sequentially through time. Our simulations show that the proposed approach can provide accurate reconstruction of a LiB cell's temperature field with a small number of sensors.**

I. Introduction

Recent technological advances have continuously pushed up the specific energy of lithium-ion batteries (LiBs) and driven down their cost. However, concerns over their thermal safety remain strong in the wake of a few high-profile fire incidents. The primary cause of LiB fires is thermal runaway, which occurs mostly in cases of abnormal heating or excessively high ambient temperature [1]. The thermal state also plays an important role in a LiB cell's capacity, voltage and cycle life other than safety, which is why LiBs usually must operate between $-10\sim50^{\circ}\mathrm{C}$ [2]. Real-time thermal monitoring is thus crucial to improving the operating safety and performance of LiBs.

This problem has attracted a growing body of research due to its significance. Most of the existing studies rest on the use of physics-based thermal models. Lumped modeling has emerged as a popular approach in this regard because of its computational efficiency. The study in [3] develops an equivalent circuit model to capture the lumped thermal dynamics at the surface and core of a cylindrical cell. Further, more sophisticated thermal circuit networks have found them useful for modeling pouch-type cells and battery packs [4]–[6]. Although computationally fast, the lumped models sacrifice fidelity and often struggle to capture the spatially non-uniform and variable temperature distribution of LiB cells or packs. To estimate the spatial non-uniformity, several works study the temperature estimation problem with two or three-dimensional thermal models derived from the energy balance equation proposed by [7]. In [8], a two-dimensional thermal model is considered to estimate a pouch cell's surface temperature distribution. In [9], a temperature-dependent impedance model is developed from a two-dimensional thermal model to estimate the temperature distribution of cylindrical cells. In [10, 11], a three-dimensional thermal model is constructed to estimate the temperature distribution of a LiB pack composed of prismatic cells. Note that a related line of research is coupling a thermal model with an electrochemical model to achieve finer-resolution thermal modeling [12]–[14]. The obtained models will require expensive computation even though they have high predictive accuracy. This makes them less suitable for real-time thermal monitoring.

However, there are two challenges in using physical models for LiB thermal monitoring. First, accurate physical modeling is hard to develop due to time-consuming analysis and validation, and even if a model is developed, it is not possible to fully capture the factors that affect the thermal behaviors of a LiB cell or system. Second, it can often be difficult to determine the parameters of a physical model, and tedious experiments or empirical guesses may become necessary [15]. Parameter drifts due to aging or changes in ambient conditions will further add to the difficulty.

Alternative to physical modeling, spatio-temporal statistical modeling and estimation have gained increasing use in describing and predicting complex systems or processes with both spatially distributed and temporally evolving dynamics. The essence of this approach lies in characterizing a spatio-temporal process of interest as a random field, in which the variations in time and space are captured by its mean and covariance models. Based on the random field, the Bayesian method can be employed for estimation when measurements arrive. Specifically, in the classical Kriging approach, spatial processes modeled as Gaussian random fields are estimated by computing the posterior Gaussian distributions [16]. For spatial fields that evolve over time, a spatio-temporal Kriging approach named Kriged Kalman filter (KKF) has proven useful [17]–[19]. The spatio-temporal statistical modeling and estimation approach has many successful applications, such as monitoring air pollutant levels and sea surface temperature [20]. However, this approach has attracted little attention in the field of battery research.

The goal of this paper is to develop a data-driven but physically meaningful approach to estimate the temperature distribution of a LiB cell in real time. We will consider a

[1]Hao Tu and Huazhen Fang are with the Department of Mechanical Engineering, University of Kansas, Lawrence, KS 66045, USA. tuhao@ku.edu, fang@ku.edu

[2]Yebin Wang is with the Mitsubishi Electric Research Laboratories, Cambridge, MA 02139, USA. yebinwang@ieee.org

[3]Xianglin Li is with the Department of Mechanical Engineering & Materials Science, Washington University, St. Louis, MO 63130, USA. lxianglin@wustl.edu

pouch-type LiB cell for the purpose of illustration, even though the approach can be generalized to LiBs of other types. We summarize our contributions as follows.

- We translate a pouch-type LiB cell's thermal model based on heat transfer principles into a spatio-temporal random field. This leads to a statistically sound but physically consistent representation of the cell's thermal process. Further, with a data-driven nature, the representation allows to make sense of data to capture uncertainties that evade physical modeling.
- We apply the KKF to predict and track the evolution of the spatio-temporal random field using real-time measurement data. As such, the cell's temperature field is reconstructed to enable effective thermal monitoring.

This paper is organized as follows. Section II presents the physical thermal model for pouch cells and its solution. In Section III, we formulate a spatial-temporal random temperature field based on the solution in Section II. Then, we present the thermal monitoring scheme of the field via the KKF. We also provide a brief overview of the field's parameter estimation procedure. Later, Section IV shows our simulation validation. Finally, Section V presents our conclusions and future research directions.

II. Thermal Model of Pouch-Type LiB Cells and Its Solution

This section introduces a two-dimensional thermal model of pouch-type LiB cells and its analytical solution. It provides a physical basis for the subsequent derivation of the pouch cell's spatio-temporal random temperature field.

A. Thermal Model of a LiB Pouch Cell

We consider a LiB pouch cell as shown in Fig. 1, which has dimensions of $L_1 \times L_2 \times L_3$ along the x_1, x_2 and x_3 axes. Because $L_3 \ll L_1, L_2$, the cell's heat transfer behavior along the x_3 axis is negligible. By contrast, the thermal dynamics in the x_1-x_2 plane is more intense and complex. Hence, we focus on only the electrode domain to develop a parsimonious but physically coherent two-dimensional thermal model. According to the energy balance principle, the temperature field within the electrode domain evolves along a two-dimensional heat diffusion equation [21]:

$$\rho c_p \frac{\partial \tilde{T}}{\partial t} = k\left(\frac{\partial^2 \tilde{T}}{\partial x_1^2} + \frac{\partial^2 \tilde{T}}{\partial x_2^2}\right) - \frac{2}{L_3} h\tilde{T} + \dot{q}, \tag{1}$$

where $\tilde{T} = T - T_\infty$ is the temperature difference between the cell and environment, ρ is the cell's mass density, c_p is the specific heat, k is the thermal conductivity, h is the convection coefficient. On the right-hand side of (1), the first term is due to the heat conduction along the x_1-x_2 plane. The second term results from the volumetric heat removal due to convection on the cell's surfaces. The third term, $\dot{q}$, is the volumetric heat generation rate in the cell which follows

$$\dot{q} = \frac{I^2(t) R_e}{V} w(x_1, x_2),$$

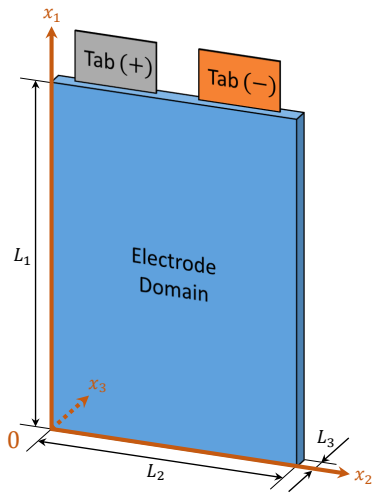

Fig. 1: Schematic diagram of a pouch-type LiB cell.

where $V = L_1 L_2 L_3$ is the cell's volume, I is the applied current, and R_e is the cell's internal resistance. Here, we only consider the Joule heat since it is the main heating source of the LiB, but other heat sources, such as entropic heat [22], are also possible to be included in the model. Furthermore, a weight function $w(x_1, x_2)$ is introduced to capture the cell's nonuniform heat generation in the x_1-x_2 plane [8].

Next, we take into account the process noise that exists in the thermal dynamics of the LiB pouch cell. To simplify notation, we will denote $\mathbf{x} = (x_1, x_2)$ and $\mathbf{x}' = (x_1', x_2')$ as two locations within the cell's electrode domain $\mathcal{L}^2$, and t, t' denote two time instants. The thermal noise is usually modeled as a white noise process W with zero mean and covariance

$$\mathrm{Cov}\left(W(\mathbf{x}, t), W(\mathbf{x}', t')\right) = \delta(t - t') Q_W(\mathbf{x}, \mathbf{x}'),$$

where $\delta(\cdot)$ is the Dirac delta function [23]. This indicates W is uncorrelated in time. Adding this noise term and reformulating the equation, (1) becomes a stochastic partial differential equation

$$\frac{\partial \tilde{T}}{\partial t} = a\left(\frac{\partial^2 \tilde{T}}{\partial x_1^2} + \frac{\partial^2 \tilde{T}}{\partial x_2^2}\right) - b\tilde{T} + c\dot{q} + W, \tag{2}$$

where $a = k/(\rho c_p)$, $b = 2h/(\rho c_p L_3)$, $c = 1/(\rho c_p)$.

Finally, we include the convective boundary conditions on the four edges of the cell's rectangular region as

$$\frac{\partial \tilde{T}}{\partial x_1} - \frac{h}{k}\tilde{T} = 0 \quad \text{at} \quad x_1 = 0, \tag{3a}$$

$$\frac{\partial \tilde{T}}{\partial x_1} + \frac{h}{k}\tilde{T} = 0 \quad \text{at} \quad x_1 = L_1, \tag{3b}$$

$$\frac{\partial \tilde{T}}{\partial x_2} - \frac{h}{k}\tilde{T} = 0 \quad \text{at} \quad x_2 = 0, \tag{3c}$$

$$\frac{\partial \tilde{T}}{\partial x_2} + \frac{h}{k}\tilde{T} = 0 \quad \text{at} \quad x_2 = L_2. \tag{3d}$$

The initial condition is given by a Gaussian process prior

$$\tilde{T}(\mathbf{x}, t_0) \sim \mathcal{GP}(m_0(\mathbf{x}), C_0(\mathbf{x}, \mathbf{x}')). \tag{4}$$

The initial-boundary value problem (IBVP) set by (2)-(4) presents a description of the thermal dynamics of a pouch-type LiB cell from the physical perspective.

B. Analytical Solution

Here, we present the analytical solution to the IBVP problem formulated in Section II-A. The solution of the IBVP can be expressed via the integral transform of the Green's function [24]. It follows that

$$\begin{aligned}\tilde{T}(\mathbf{x}, t) = &\iint_{\mathcal{L}^2} \tilde{T}(\mathbf{x}', s) G(\mathbf{x}, \mathbf{x}', t-s)\, d\mathbf{x}' \\ &+ \int_s^t \iint_{\mathcal{L}^2} c\dot{q}(\mathbf{x}', \tau) G(\mathbf{x}, \mathbf{x}', t-\tau)\, d\mathbf{x}' d\tau \\ &+ \int_s^t \iint_{\mathcal{L}^2} W(\mathbf{x}', \tau) G(\mathbf{x}, \mathbf{x}', t-\tau)\, d\mathbf{x}' d\tau,\end{aligned}$$

where $G(\mathbf{x}, \mathbf{x}', \cdot)$ is the Green's function of the IBVP problem, t and $s < t$ are two arbitrary time instants. Here, the third term on the right-hand side is a Gaussian process with zero mean and covariance function [23]

$$\begin{aligned}Q_\eta(\mathbf{x}, \mathbf{x}'; t-s) = &\int_s^t \iint_{\mathcal{L}^2} G(\mathbf{x}', \mathbf{y}', t-\tau) \\ &\iint_{\mathcal{L}^2} G(\mathbf{x}, \mathbf{y}, t-\tau) Q_W(\mathbf{y}, \mathbf{y}')\, d\mathbf{y}\, d\mathbf{y}'\, d\tau.\end{aligned}$$

If considering the time range $(t_{k-1}, t_k]$ from the $k-1$-th to the k-th discrete time instants, we can exactly express the solution at t_k as the following discrete-time model

$$\begin{aligned}\tilde{T}(\mathbf{x}, t_k) = &\iint_{\mathcal{L}^2} \tilde{T}(\mathbf{x}', t_{k-1}) G(\mathbf{x}, \mathbf{x}'; \Delta t_k)\, d\mathbf{x}' \\ &+ \int_{t_{k-1}}^{t_k} \iint_{\mathcal{L}^2} c\dot{q}(\mathbf{x}', t_{k-1}) G(\mathbf{x}, \mathbf{x}', t_k - \tau)\, d\mathbf{x}' d\tau \\ &+ \eta(\mathbf{x}, t_k),\end{aligned} \tag{5}$$

where $\Delta t_k = t_k - t_{k-1}$ is the time interval, and $\eta(\mathbf{x}, t_k) \sim \mathcal{GP}(0, Q_\eta(\mathbf{x}, \mathbf{x}'; \Delta t_k))$. Note that, throughout the paper, we consider Δt_k to be known and fixed, and $\dot{q}(\mathbf{x}, t_{k-1})$ does not change within Δt_k. In this case, $\eta(\mathbf{x}, t_k)$ becomes a Gaussian process which is uncorrelated in time.

The solution (5) shows the time evolution of a pouch cell's temperature field from a physical perspective. It contains thermal parameters which must be estimated by physical experiments. In reality, there may still exist uncaptured dynamics which harm its accuracy.

III. The KKF

In this section, we construct a spatio-temporal random temperature field for pouch cells based on the solution in (5). Then, we will introduce a monitoring scheme of the temperature field using the KKF. Finally, we provide an overview of the parameter estimation of the field.

A. Spatio-Temporal Random Field

The method taken in [17, 18] expresses $\tilde{T}(\mathbf{x}, t_k)$ through an expansion of a set of complete and orthonormal basis functions $\{\phi_i(\mathbf{x})\}_{i=1}^\infty$ on $\mathcal{L}^2$

$$\tilde{T}(\mathbf{x}, t_k) = \sum_{i=1}^\infty \alpha_i(t_k) \phi_i(\mathbf{x}),$$

where $\alpha_i(t_k)$ is a random time series for each $i \in \{1, 2, ...\}$. Due to completeness, we can also expand the Green's function as follows:

$$G(\mathbf{x}, \mathbf{x}'; \Delta t_k) = \sum_{l=1}^\infty \beta_l(\mathbf{x}) \phi_l(\mathbf{x}'),$$

where $\{\beta_l(\mathbf{x})\}_{l=1}^\infty$ are some functions of $\mathbf{x}$. Note that $\int_{t_{k-1}}^{t_k} G(\mathbf{x}, \mathbf{x}', t_k - \tau)\, d\tau = \int_0^{\Delta t_k} G(\mathbf{x}, \mathbf{x}', \zeta)\, d\zeta$. Then, by truncating the infinite series and using the orthonormality of the basis functions, we can rewrite (5) as (6), where

$$\kappa(\mathbf{x}) = (cR_e/V) \iint_{\mathcal{L}^2} w(\mathbf{x}') \int_0^{\Delta t_k} G(\mathbf{x}, \mathbf{x}', \zeta)\, d\zeta\, d\mathbf{x}'$$

is a function of $\mathbf{x}$, and

$$\begin{aligned}\boldsymbol{\alpha}(t_k) &= (\alpha_1(t_k), ..., \alpha_N(t_k))^\top \in \mathbb{R}^N, \\ \boldsymbol{\beta}(\mathbf{x}) &= (\beta_1(\mathbf{x}), ..., \beta_N(\mathbf{x}))^\top \in \mathbb{R}^N, \\ \boldsymbol{\phi}(\mathbf{x}) &= (\phi_1(\mathbf{x}), ..., \phi_N(\mathbf{x}))^\top \in \mathbb{R}^N.\end{aligned}$$

To compensate for the truncation errors and to deal with spatial uncertainties not included in $\tilde{T}(\mathbf{x}, t_k)$, we introduce a Gaussian process $\nu(\mathbf{x}, t_k)$ with zero mean and covariance

$$\mathrm{Cov}\,(\nu(\mathbf{x}, t), \nu(\mathbf{x}', t')) = \delta(t - t') Q_\nu(\mathbf{x}, \mathbf{x}').$$

It captures small-scale spatial variability but does not have temporal dynamics. Then, the predictive distribution of the temperature at any location $\mathbf{x}$ is given by

$$\begin{aligned}Y(\mathbf{x}, t_k) &= \tilde{T}(\mathbf{x}, t_k) + \nu(\mathbf{x}, t_k) \\ &= \boldsymbol{\phi}^\top(\mathbf{x}) \boldsymbol{\alpha}(t_k) + \nu(\mathbf{x}, t_k).\end{aligned} \tag{7}$$

Considering sensors are placed at M locations $\{s_1, ..., s_M\}$ of the pouch cell to collect measurements, we can write down the evolution of the coefficient vector $\boldsymbol{\alpha}(t_k)$ as

$$\boldsymbol{\alpha}(t_k) = \bar{\boldsymbol{A}} \boldsymbol{\alpha}(t_{k-1}) + \bar{\boldsymbol{B}} I^2(t_{k-1}) + \bar{\boldsymbol{\eta}}(t_k), \tag{8}$$

where $\boldsymbol{J} = (\boldsymbol{\Phi}^\top \boldsymbol{\Phi})^{-1} \boldsymbol{\Phi}^\top$, $\bar{\boldsymbol{B}} = \boldsymbol{J}\boldsymbol{K}$, $\bar{\boldsymbol{A}} = \boldsymbol{J}\boldsymbol{B}$, $\bar{\boldsymbol{\eta}}(t_k) = \boldsymbol{J}\boldsymbol{\eta}(t_k)$, and

$$\begin{aligned}\boldsymbol{\Phi} &= [\phi(s_1), ..., \phi(s_M)]^\top \in \mathbb{R}^{M \times N}, \\ \boldsymbol{B} &= [\beta(s_1), ..., \beta(s_M)]^\top \in \mathbb{R}^{M \times N}, \\ \boldsymbol{K} &= (\kappa(s_1), ..., \kappa(s_M))^\top \in \mathbb{R}^M, \\ \boldsymbol{\eta}(t_k) &= (\eta(s_1, t_k), ..., \eta(s_M, t_k))^\top \in \mathbb{R}^M.\end{aligned}$$

For the M sensor locations, the noisy measurement vector is given by

$$\begin{aligned}\boldsymbol{Z}(t_k) &= \boldsymbol{Y}(t_k) + \boldsymbol{\epsilon}(t_k) \\ &= \boldsymbol{\Phi}\boldsymbol{\alpha}(t_k) + \boldsymbol{\nu}(t_k) + \boldsymbol{\epsilon}(t_k),\end{aligned} \tag{9}$$

$$
\begin{aligned}
\tilde{T}(\mathbf{x}, t_k) &= \boldsymbol{\phi}(\mathbf{x})^\top \boldsymbol{\alpha}(t_k) \\
&= \iint_{\mathcal{L}^2} \left(\sum_{i=1}^{N} \alpha_i(t_{k-1}) \phi_i(\mathbf{x}') \right) \left(\sum_{l=1}^{N} \beta_l(\mathbf{x}) \phi_l(\mathbf{x}') \right) d\mathbf{x}' + \iint_{\mathcal{L}^2} \left(\frac{cI^2(t_{k-1}) R_e}{V} w(\mathbf{x}') \right) \left(\int_0^{\Delta t_k} G(\mathbf{x}, \mathbf{x}', \zeta)\, d\zeta \right) d\mathbf{x}' \\
&\quad + \eta(\mathbf{x}, t_k) \\
&= \boldsymbol{\beta}(\mathbf{x})^\top \boldsymbol{\alpha}(t_{k-1}) + \kappa(\mathbf{x}) I^2(t_{k-1}) + \eta(\mathbf{x}, t_k)
\end{aligned} \tag{6}
$$

where $\boldsymbol{\epsilon}(t_k) \sim \mathcal{N}(\mathbf{0}, \sigma^2 \boldsymbol{I}_{M\times M}) \in \mathbb{R}^M$ is the white Gaussian measurement noise, $\boldsymbol{I}_{M\times M} \in \mathbb{R}^{M\times M}$ is the identity matrix, and

$$
\begin{aligned}
\boldsymbol{Z}(t_k) &= (Z(s_1, t_k), ..., Z(s_M, t_k))^\top \in \mathbb{R}^M, \\
\boldsymbol{Y}(t_k) &= (Y(s_1, t_k), ..., Y(s_M, t_k))^\top \in \mathbb{R}^M, \\
\boldsymbol{\nu}(t_k) &= (\nu(s_1, t_k), ..., \nu(s_M, t_k))^\top \in \mathbb{R}^M.
\end{aligned}
$$

Up to this point, we have formulated a spatio-temporal random field $Y(\mathbf{x}, t_k)$ to represent the LiB pouch cell's thermal process. This statistical representation is data-driven in nature but physically consistent. Its mean $\tilde{T}(\mathbf{x}, t_k)$ is a linear combination of some known basis functions $\boldsymbol{\phi}(\mathbf{x})$ with the coefficient $\boldsymbol{\alpha}(t_k)$ evolving in time according to (8). In addition, the term $\nu(\mathbf{x}, t_k)$ captures some small-scale uncertainties that $\tilde{T}(\mathbf{x}, t_k)$ does not take into account. We can use a random field setup in the form of $Y(\mathbf{x}, t_k)$ to track the time evolution of a pouch cell's temperature field. Here, we highlight two points. First, $Y(\mathbf{x}, t_k)$ is continuous in space and discrete in time. This form allows the reconstructed temperature field to have a high spatial resolution. Second, the dimension of $\boldsymbol{\alpha}(t_k)$ is the same as the number of chosen $\boldsymbol{\phi}(\mathbf{x})$, providing flexibility for balancing the computational efficiency and accuracy of the model.

B. Spatio-Temporal Monitoring of the Field

Taking a Bayesian probability perspective, the spatio-temporal monitoring of the temperature field in real time boils down to compute the posterior distribution of $Y(\mathbf{x}, t_k)$ conditioned on the up-to-date measurements $\boldsymbol{Z}(t_{1:k}) := \{\boldsymbol{Z}(t_1), ..., \boldsymbol{Z}(t_k)\}$. It can be done in two steps. The first one is to sequentially estimate $\boldsymbol{\alpha}(t_k)$ using the up-to-date measurements; the second one is to do Bayesian universal Kriging [25].

The linear state-space model in (8)-(9) demonstrates the temporal evolution of $\boldsymbol{\alpha}(t_k)$ and the measurements at different sensor locations. Given this model, an optimal estimate of $\boldsymbol{\alpha}(t_k)$ can be computed sequentially here using the well-known Kalman filter. It consists of two steps.

Step 1 - Prediction: Computing $\boldsymbol{\alpha}(t_k) \mid \boldsymbol{Z}(t_{1:k-1})$ which follows a normal distribution with mean

$$
\begin{aligned}
\hat{\boldsymbol{\alpha}}(t_k \mid t_{1:k-1}) &\coloneqq \mathrm{E}\left(\boldsymbol{\alpha}(t_k) \mid \boldsymbol{Z}(t_{1:k-1})\right) \\
&= \bar{\boldsymbol{A}} \hat{\boldsymbol{\alpha}}(t_{k-1} \mid t_{1:k-1}) + \bar{\boldsymbol{B}} I^2(t_{k-1})
\end{aligned}
$$

and covariance

$$
\begin{aligned}
\boldsymbol{\Sigma}(t_k \mid t_{1:k-1}) &\coloneqq \mathrm{Cov}\left(\boldsymbol{\alpha}(t_k) \mid \boldsymbol{Z}(t_{1:k-1})\right) \\
&= \bar{\boldsymbol{A}} \boldsymbol{\Sigma}(t_{k-1} \mid t_{1:k-1}) \bar{\boldsymbol{A}}^\top + \boldsymbol{Q}_{\bar{\boldsymbol{\eta}}},
\end{aligned}
$$

where $\boldsymbol{Q}_{\bar{\boldsymbol{\eta}}} \coloneqq \mathrm{Cov}(\bar{\boldsymbol{\eta}}(t_k)) \in \mathbb{R}^{N\times N}$.

Step 2 - Update: Calculating $\boldsymbol{\alpha}(t_k) \mid \boldsymbol{Z}(t_{1:k})$ which is a normal distribution with mean

$$
\begin{aligned}
\hat{\boldsymbol{\alpha}}(t_k \mid t_{1:k}) &\coloneqq \mathrm{E}\left(\boldsymbol{\alpha}(t_k) \mid \boldsymbol{Z}(t_{1:k})\right) \\
&= \hat{\boldsymbol{\alpha}}(t_k \mid t_{1:k-1}) \\
&\quad + \boldsymbol{G}_{\boldsymbol{K}}(t_k) \left(\boldsymbol{Z}(t_k) - \boldsymbol{\Phi} \hat{\boldsymbol{\alpha}}(t_k \mid t_{1:k-1})\right)
\end{aligned}
$$

and covariance

$$
\begin{aligned}
\boldsymbol{\Sigma}(t_k \mid t_{1:k}) &\coloneqq \mathrm{Cov}\left(\boldsymbol{\alpha}(t_k) \mid \boldsymbol{Z}(t_{1:k})\right) \\
&= \boldsymbol{\Sigma}(t_k \mid t_{1:k-1}) - \boldsymbol{G}_{\boldsymbol{K}}(t_k) \boldsymbol{\Phi} \boldsymbol{\Sigma}(t_k \mid t_{1:k-1}),
\end{aligned}
$$

where $\boldsymbol{G}_{\boldsymbol{K}}(t_k)$ is the Kalman gain given by

$$
\boldsymbol{G}_{\boldsymbol{K}}(t_k) = \boldsymbol{\Sigma}(t_k \mid t_{1:k-1}) \boldsymbol{\Phi}^\top \left(\boldsymbol{\Phi} \boldsymbol{\Sigma}(t_k \mid t_{1:k-1}) \boldsymbol{\Phi}^\top + \boldsymbol{V}_\sigma \right)^{-1}.
$$

Here, $\boldsymbol{V}_\sigma = \boldsymbol{Q}_{\boldsymbol{\nu}} + \sigma^2 \boldsymbol{I}_{M\times M} \in \mathbb{R}^{M\times M}$, $\boldsymbol{Q}_{\boldsymbol{\nu}} := \mathrm{Cov}(\boldsymbol{\nu}(t_k)) = [Q_\nu(s_i, s_j)] \in \mathbb{R}^{M\times M}$.

Given the sequentially estimated coefficient $\hat{\boldsymbol{\alpha}}(t_k \mid t_{1:k})$, the covariance $\boldsymbol{\Sigma}(t_k \mid t_{1:k})$ and the random field in (7), the posterior predictive distribution $p\left(Y(\mathbf{x}, t_k) \mid \boldsymbol{Z}\right)(t_{1:k}))$ of the temperature field at any time instant t_k and location $\mathbf{x}$ can then be determined via the Bayesian universal Kriging. The result follows a normal distribution with mean (10) and covariance (11), where $\boldsymbol{\Gamma}(\mathbf{x}) = (Q_\nu(\mathbf{x}, s_1), ..., Q_\nu(\mathbf{x}, s_M))^\top \in \mathbb{R}^M$. In the sense of minimum mean squared error, the optimal estimator of $Y(\mathbf{x}, t_k)$ is the mean $\hat{Y}(\mathbf{x}, t_k \mid t_{1:k})$ of the posterior distribution, and the covariance $\Sigma_Y(\mathbf{x}, t_k \mid t_{1:k})$ characterizes the confidence of this estimation.

C. Parameter Estimation of the Field

Successful spatio-temporal monitoring of the LiB cell requires the parameters of the random field to be known. The basic parameters and functions are summarized as $\{\bar{\boldsymbol{A}}, \bar{\boldsymbol{B}}, \boldsymbol{Q}_{\bar{\boldsymbol{\eta}}}, \boldsymbol{\phi}(\mathbf{x}), Q_\nu(\mathbf{x}, \mathbf{x}'), \sigma^2, \mu_0, \Sigma_0\}$, where μ_0 and Σ_0 are the mean and covariance of the initial coefficient $\boldsymbol{\alpha}(t_0)$, respectively. Other matrices in Section III-B can be determined from the $\boldsymbol{\phi}(\mathbf{x})$, $Q_\nu(\mathbf{x}, \mathbf{x}')$ and σ^2 above. Here, the choice of basis functions $\boldsymbol{\phi}(\mathbf{x})$ is not unique, as long as they are complete and orthonormal on $\mathcal{L}^2$. For other parameters and functions, they can be identified purely based on a time-series temperature data $\boldsymbol{Z}(t_{1:T})$ collected at M locations and

$$\hat{Y}(\mathbf{x}, t_k \mid t_{1:k}) \coloneqq \mathrm{E}\left(Y(\mathbf{x}, t_k) \mid \boldsymbol{Z}(t_{1:k})\right) = \boldsymbol{\phi}(\mathbf{x})^\top \hat{\boldsymbol{\alpha}}(t_k \mid t_{1:k}) + \boldsymbol{\Gamma}(\mathbf{x})^\top \boldsymbol{V}_\sigma^{-1} \left(\boldsymbol{Z}(t_k) - \boldsymbol{\Phi}\hat{\boldsymbol{\alpha}}(t_k \mid t_{1:k})\right) \tag{10}$$

$$\begin{aligned}\Sigma_Y(\mathbf{x}, t_k \mid t_{1:k}) &\coloneqq \mathrm{Cov}\left(Y(\mathbf{x}, t_k) \mid \boldsymbol{Z}(t_{1:k})\right) \\ &= Q_\nu(\mathbf{x}, \mathbf{x}) - \boldsymbol{\Gamma}(\mathbf{x})^\top \boldsymbol{V}_\sigma^{-1} \boldsymbol{\Gamma}(\mathbf{x}) + \left(\boldsymbol{\phi}(\mathbf{x}) - \boldsymbol{\Phi}^\top \boldsymbol{V}_\sigma^{-1} \boldsymbol{\Gamma}(\mathbf{x})\right)^\top \boldsymbol{\Sigma}(t_k \mid t_{1:k}) \left(\boldsymbol{\phi}(\mathbf{x}) - \boldsymbol{\Phi}^\top \boldsymbol{V}_\sigma^{-1} \boldsymbol{\Gamma}(\mathbf{x})\right)\end{aligned} \tag{11}$$

T time intervals from the LiB cell. Specifically, we follow a two-level hierarchical procedure.

The first level focuses on the identification of σ^2 and $Q_\nu(\mathbf{x}, \mathbf{x}')$. The measurement error σ^2 can be obtained from the properties of the temperature sensor used. If such information is not available, σ^2 can also be estimated together with the spatial covariance function $Q_\nu(\mathbf{x}, \mathbf{x}')$ through their relation with the empirical variogram of the data. Interested readers are referred to [20] for a detailed description of the empirical variogram. Note that one assumption we can make is that ν is an isotropic process, i.e., $Q_\nu(\mathbf{x}, \mathbf{x}') = K_\nu(\|\mathbf{x} - \mathbf{x}'\|)$ for some function K_ν. This assumption is valid since the dimensions of pouch cells are small enough.

The second level deals with the remaining parameters, i.e., $\theta = \{\bar{\boldsymbol{A}}, \bar{\boldsymbol{B}}, \boldsymbol{Q}_{\bar{\boldsymbol{\eta}}}, \mu_0, \Sigma_0\}$. An effective approach is the maximum likelihood estimation, which boils down to solving the maximization problem as follows:

$$\hat{\theta} = \arg\max_\theta L_\theta(\boldsymbol{Z}(t_{1:T})) \coloneqq \log p_\theta(\boldsymbol{Z}(t_{1:T})),$$

where $p_\theta(\boldsymbol{Z}(t_{1:T}))$ is the joint density or likelihood of the data and $L_\theta\left(\boldsymbol{Z}(t_{1:T})\right)$ is the log-likelihood. A number of methods are available to find $\hat{\theta}$ for linear state-space models. The expectation-maximization (EM) algorithm is used in this paper due to its conceptually simple procedure [26, 27].

Remark 1: For the sake of coherence and clarity, we consider the same M sensors in Section III-B and III-C. However, the number and location of the sensors do not have to be the same. Specifically, one may collect data from more locations in the parameter estimation stage to obtain an accurate model, while only applying a small number of sensors when estimating the temperature field of a LiB pouch cell. Correspondingly, the dimension and computational costs of matrices $\boldsymbol{V}_\sigma$, $\boldsymbol{\Gamma}(\mathbf{x})$, and $\boldsymbol{\Phi}$ are reduced. This is a valuable feature since in practice the number of sensors available when performing temperature estimation may be limited. We will demonstrate this strategy in Section IV.

IV. Simulation Validation

The previous sections illustrate our proposed method for the temperature field estimation of pouch-type LiB cells via KKF. In this section, a simulation is provided to show the effectiveness of this method.

A. Simulation Settings

We consider a $\mathrm{LiMn_2O_4}$ pouch cell as used in [12]. The cell has a capacity of 14.6 Ah and dimensions of 192×145×5.4 mm. We perform a CFD simulation of the cell's thermal and electrochemical behavior using the ANSYS Fluent package to generate the ground truth dataset. In the CFD simulation, we mesh the electrode domain into a 20×17 grid. The environmental temperature is set to 300 K.

The selection of the sensor locations and the current profiles are critical. A rule of thumb is to make them broadly cover the pouch cell's electrode domain. Here, we select 18 (16 black and 2 red asterisks in Figs. 5a-5d) of the 20×17 grid nodes and place sensors on them. In the training (parameter estimation) phase, the data collected by all sensors are used. However, only the sensors placed on the two red asterisks are used during the testing (KKF-based thermal monitoring) phase. The current profile to generate the training data should be chosen such that it covers the cell's operating current and temperature range well. In our simulation, the training data are generated by applying a 5 C constant discharging current to the cell. Then, we test the KKF using a data set generated by a modified US06 [28] profile shown in Fig. 2.

B. Simulation Results

We apply the 5 C discharging current to the cell for 670 seconds. The data collected from the 18 sensors are used for model training. The measurement is assumed to be noise-free since the data are generated by the CFD simulation. Besides, we use a set of 11 complete and orthonormal basis functions $\boldsymbol{\phi}(\mathbf{x})$. Now, based on the hierarchical procedure in Section III-C, the first step is the identification of the covariance function K_ν. We consider the squared-exponential kernel. Fig. 3 illustrates the identified K_ν. As expected, the covariance between two locations decreases as their distance increases. We can then determine the covariance matrix and the measurement matrix based on this empirical covariance function. Finally, we estimate the parameter set θ in Section III-C by maximizing the log-likelihood function $L_\theta(\boldsymbol{Z}(t_{1:T}))$ via the EM algorithm. We run the EM algorithm for 10 iterations. Fig. 4 shows the change in log-likelihood value. As expected, the value increases with the number of iterations.

With the model identified above, the temperature field of the pouch cell can be estimated by running the KKF in Section III-B. Only the two sensors located at the red asterisks are used here. The KKF can provide accurate temperature estimation. Under the US06 testing profiles, the maximum absolute estimation errors for all locations and all time instants is 1.01 K. Further, Figs. 5a-5d show the comparison of the true and the estimated temperature field when the modified US06 current profile is applied to the cell. The first row illustrates the true temperature field at different time instants. The temperature increases through time due to the heat generation in charging/discharging, with

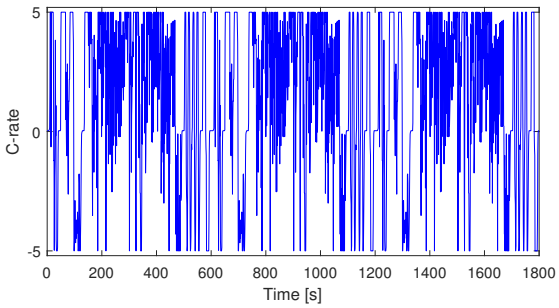

Fig. 2: Modified US06 current profile.

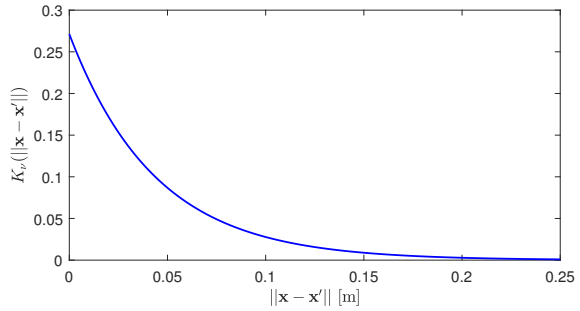

Fig. 3: Identified empirical covariance function.

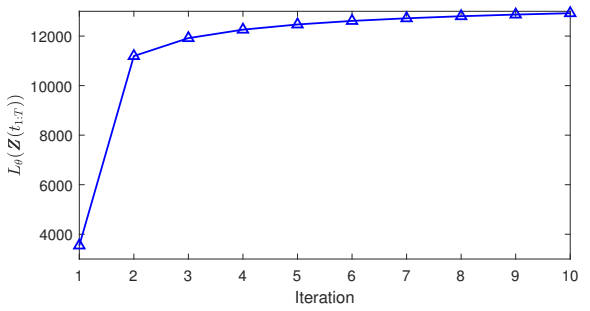

Fig. 4: EM iterations for maximum likelihood estimation.

its spatial non-uniformity growing. The second row shows the temperature field estimated by the KKF at different time instants. It has great accuracy compared to the truth, despite the use of only two sensors. It is worth mentioning that our simulations show that an increase in estimation accuracy can be expected in two ways. First, we can use more sensors during the training phase, as placing sensors at more locations can provide more information about the temperature field. Second, we can increase the number of basis functions when constructing the model, which leads to a coefficient vector $\boldsymbol{\alpha}(t_k)$ of a higher dimension, though the computational cost will also increase accordingly.

V. Conclusions

Effective thermal monitoring is essential for the safety and performance of LiBs in their operation. In this paper, we study the spatio-temporal temperature field estimation for LiB based on a data-driven approach named KKF. Starting from the heat transfer principles, we uniquely show that the temperature evolution of a pouch cell can be formulated as a spatio-temporal random field with physical consistentency. The parameters of the field are fully determined by the data collected from temperature sensors according to a hierarchical scheme. Leveraging the spatio-temporal random field, the KKF is applied to estimate the temperature field when the measurements come sequentially. Our simulation demonstrates that the approach can provide accurate temperature estimation for LiB using a small number of sensors. Our future work will include experimental validation of the KKF approach and investigate its application to various LiB thermal management tasks.

References

[1] Q. Wang, P. Ping, X. Zhao, G. Chu, J. Sun, and C. Chen, "Thermal runaway caused fire and explosion of lithium ion battery," *Journal of Power Sources*, vol. 208, pp. 210–224, 2012.

[2] T. M. Bandhauer, S. Garimella, and T. F. Fuller, "A critical review of thermal issues in lithium-ion batteries," *Journal of The Electrochemical Society*, vol. 158, no. 3, p. R1, 2011.

[3] X. Lin, H. E. Perez, J. B. Siegel, A. G. Stefanopoulou, Y. Li, R. D. Anderson, Y. Ding, and M. P. Castanier, "Online parameterization of lumped thermal dynamics in cylindrical lithium ion batteries for core temperature estimation and health monitoring," *IEEE Transactions on Control Systems Technology*, vol. 21, no. 5, pp. 1745–1755, 2013.

[4] Y. Xiao, "Model-based virtual thermal sensors for lithium-ion battery in EV applications," *IEEE Transactions on Industrial Electronics*, vol. 62, no. 5, pp. 3112–3122, 2015.

[5] X. Lin, H. E. Perez, J. B. Siegel, and A. G. Stefanopoulou, "Robust estimation of battery system temperature distribution under sparse sensing and uncertainty," *IEEE Transactions on Control Systems Technology*, vol. 28, no. 3, pp. 753–765, 2020.

[6] Y. Shi, K. Smith, E. Wood, and A. Pesaran, "A multi-node thermal system model for lithium-ion battery packs," in *2015 American Control Conference (ACC)*, pp. 723–727, 2015.

[7] D. Bernardi, E. Pawlikowski, and J. Newman, "A general energy balance for battery systems," *Journal of The Electrochemical Society*, vol. 132, no. 1, pp. 5–12, 1985.

[8] S. Sattarzadeh, T. Roy, and S. Dey, "Real-time estimation of 2-D temperature distribution in lithium-ion pouch cells," *IEEE Transactions on Transportation Electrification*, vol. 7, no. 4, pp. 2249–2259, 2021.

[9] R. R. Richardson, S. Zhao, and D. A. Howey, "On-board monitoring of 2-D spatially-resolved temperatures in cylindrical lithium-ion batteries: Part II. state estimation via impedance-based temperature sensing," *Journal of Power Sources*, vol. 327, pp. 726–735, 2016.

[10] N. Tian and H. Fang, "Distributed Kalman filtering-based three-dimensional temperature field reconstruction for a lithium-ion battery pack," in *2017 American Control Conference (ACC)*, pp. 905–910, 2017.

[11] N. Tian, H. Fang, and Y. Wang, "3-D temperature field reconstruction for a lithium-ion battery pack: A distributed Kalman filtering approach," *IEEE Transactions on Control Systems Technology*, vol. 27, no. 2, pp. 847–854, 2019.

[12] U. S. Kim, J. Yi, C. B. Shin, T. Han, and S. Park, "Modeling the dependence of the discharge behavior of a lithium-ion battery on the environmental temperature," *Journal of The Electrochemical Society*, vol. 158, no. 5, p. A611, 2011.

[13] S. Goutam, A. Nikolian, J. Jaguemont, J. Smekens, N. Omar, P. Van Dan Bossche, and J. Van Mierlo, "Three-dimensional electro-thermal model of Li-ion pouch cell: Analysis and comparison of cell design factors and model assumptions," *Applied Thermal Engineering*, vol. 126, pp. 796–808, 2017.

[14] A. Samba, N. Omar, H. Gualous, Y. Firouz, P. Van den Bossche, J. Van Mierlo, and T. I. Boubekeur, "Development of an advanced two-dimensional thermal model for large size lithium-ion pouch cells," *Electrochimica Acta*, vol. 117, pp. 246–254, 2014.

[15] B. Wu, Z. Li, and J. Zhang, "Thermal design for the pouch-type large-format lithium-ion batteries," *Journal of The Electrochemical Society*, vol. 162, no. 1, pp. A181–A191, 2014.

[16] N. Cressie, "The origins of Kriging," *Mathematical Geology*, vol. 22, pp. 239–252, 1990.

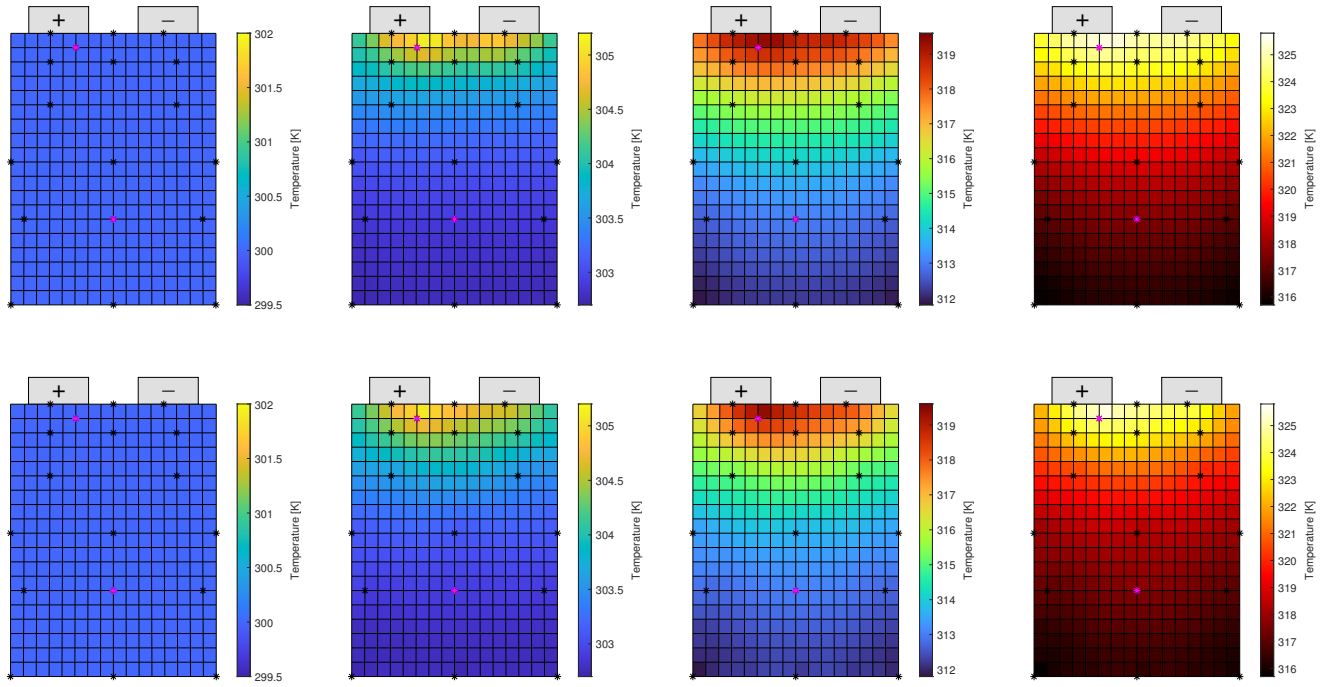

(a) t = 1 s (b) t = 200 s (c) t = 1,000 s (d) t = 1,800 s

Fig. 5: Monitoring of the pouch cell's temperature field under a modified US06 current profile. First row: the true temperature field. Second row: the estimated temperature field by the KKF approach. $*$ and $*$ denote sensor locations. The training phase uses data from all the sensors labeled as $*$ and $*$; the testing phase uses data from only two sensors labeled as $*$.

[17] K. V. Mardia, C. Goodall, E. J. Redfern, and F. J. Alonso, "The Kriged Kalman filter," *Test*, vol. 7, p. 217–282, 1998.

[18] N. Cressie and C. K. Wikle, "Space-time Kalman filter," *Encyclopedia of Environmetrics*, vol. 4, p. 2045–2049, 2002.

[19] S. Sarkka, A. Solin, and J. Hartikainen, "Spatiotemporal learning via infinite-dimensional Bayesian filtering and smoothing: A look at Gaussian process regression through Kalman filtering," *IEEE Signal Processing Magazine*, vol. 30, no. 4, pp. 51–61, 2013.

[20] N. Cressie and C. K. Wikle, *Statistics for spatio-temporal data*. Hoboken, N.J: Wiley, 2011.

[21] M. Yazdanpour, P. Taheri, A. Mansouri, and M. Bahrami, "A distributed analytical electro-thermal model for pouch-type lithium-ion batteries," *Journal of The Electrochemical Society*, vol. 161, no. 14, pp. A1953–A1963, 2014.

[22] K. E. Thomas and J. Newman, "Thermal modeling of porous insertion electrodes," *Journal of The Electrochemical Society*, vol. 150, no. 2, p. A176, 2003.

[23] S. Särkkä and A. Solin, *Applied Stochastic Differential Equations*. Cambridge University Press, 2019.

[24] A. D. Polyanin, *Handbook of Linear Partial Differential Equations for Engineers and Scientists (1st ed.)*. Chapman and Hall/CRC, 2001.

[25] J. Cortes, "Distributed Kriged Kalman filter for spatial estimation," *IEEE Transactions on Automatic Control*, vol. 54, no. 12, pp. 2816–2827, 2009.

[26] R. H. Shumway and D. S. Stoffer, "An approach to time series smoothing and forecasting using the EM algorithm," *Journal of Time Series Analysis*, vol. 3, no. 4, pp. 253–264, 1982.

[27] J. Cara, J. Juan, and E. Alarcón, "Using the EM algorithm to estimate the state space model for OMAX," in *International Conference on Noise and Vibration Engineering*, 2014.

[28] Environmental Protection Agency, "Vehicle and fuel emission testing," *Technical Report*.